Sciaky's electron beam additive manufacturing for 3D metal printing

G. Kishan*

University College of Engineering and Technology for Women, Kakatiya Univerity, Warangal, Telangana, India.

ABSTRACT

Electron beam additive manufacturing is a novel method of manufacturing parts directly from digital STL file by using layer by layer material build-up approach. This is tool less manufacturing methodology to produce fully dense metallic parts in short interval of time, with high precision. Features of additive manufacturing like freedom of part design, part complexity, light weight, part consolidation and design for function are depositing particular interests in metal additive manufacturing for aerospace, oil & gas, marine and automobile applications. This research paper presents overview of sciaky's electron beam 3D metal printing technology, materials, applications.

1. Introduction

3D printing also known as Additive manufacturing is a process of joining materials to make objects from 3D model STL file data, usually one layer over the layer, as opposed to subtractive manufacturing methodologies. This tool less manufacturing approach can give industry new design flexibility, reduce energy use and shorten time to market. Main applications of metal additive manufacturing include rapid prototyping, Parts made faster with less material waste, reduced machining time and shorter time-to-market, direct part production and part repairing of metallic materials. The two main parameters of any metal AM process are type of input raw material and energy source used to form the part (Bhavar et al., 2014). Input raw material can be used in the form of metal powder or wire whereas laser/ electron beam or arc can be used as energy source shown in the Figure 1.

Metal 3D printing processes can be broadly classified into two major groups, - Powder Bed Fusion based technologies (PBF) and Directed Energy Deposition (DED) based technologies.
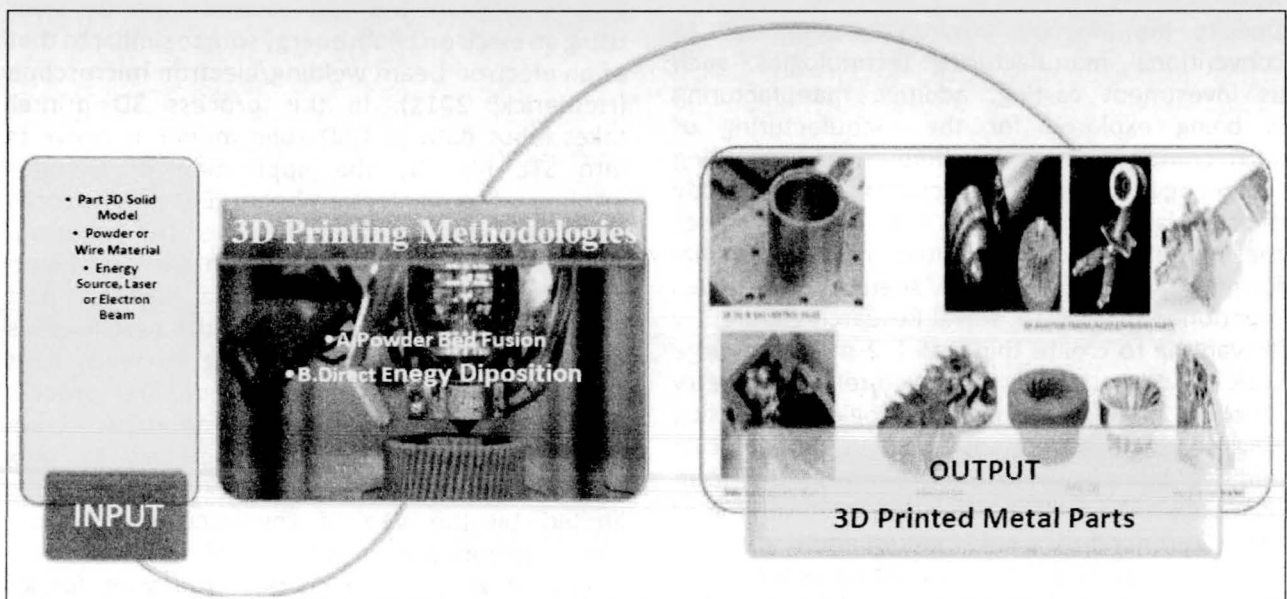

Fig. 1. 3D Metal printing process.

*Corresponding author,
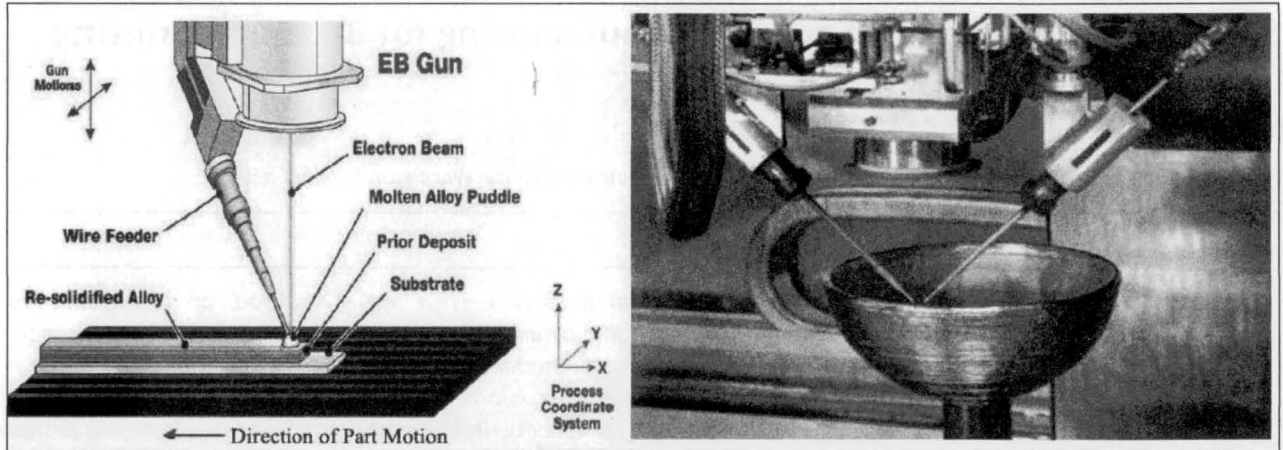E-mail: kishangucetw@gmail.com

Fig. 2. (a) Electron beam metal 3D printing process model, (b) Electron beam metal 3D printing.

Both of these technologies can be further classified based on the type of energy source used (Bhavar et al., 2014). With the addition of metallic 3D printing manufacturing technologies into the industry is of great interest currently. It can be seen by the investments made by various countries such as China, U.S. and Singapore (Sun, 2013; Anderson, 2013). Electron beam melting has a capacity of producing usable parts with high mechanical properties more rapidly and efficiently as compared to laser based metallic additive manufacturing technologies, such as selective laser melting (Chua, 2010). 3D printing of complex industrial parts such as turbine blades, pump impellers, fuel nozzles, turbocharger wheels, etc., has been carried out around the world recently (Quail et al., 2009; Lu et al., 2013). Due to the inherent advantages compared to conventional manufacturing technologies, such as investment casting, additive manufacturing is being explored for the manufacturing of such complex parts. As additive manufacturing technology matures, the challenge to directly produce large scale complex parts that surpasses the manufacturing capabilities of conventional forming processes can be seen by objectives mentioned by the U.S. Naval Research Laboratory in wanting to create thin wall (~2 mm) and large scale (~2 m) parts with complex internal geometry (Cooper, 2014). Nanyang Technological University, Singapore has also invested in large scale additive manufacturing technology in the form of Arcam A2XX EBM which has a built volume of 350 x 380 mm3 (Arcam, 2014). In addition to the advantages such as the 3D printing process and high energy efficiency, electron beam melted parts are also reported to have minimum residual stresses as compared to laser based 3D printing methodologies (Chua et al., 2010). Thus, after printing finishing and heat treatment may not be necessary for the EBM built usable parts. Moreover, EBM has no challenging issues with reflection in the molten pool, as a result that some certain materials which were not able to print by laser based processes can be manufactured easily by EBM (Chua et al., 2010). This paper explains about processing methodology of sciaky's electron beam additive manufactuing, materials, applications etc. 3D Printing is growing rapidly and had an undeniable impact on manufacturing technology.

Sciaky's electron beam additive manufacturing technology

The electron beam melting (EBM) technology uses a heated powder bed of metal in a vacuum that is then melted and formed layer by layer using an electron beam energy source similar to that of an electron beam welding/electron microscope (Herderick, 2011). In this process 3D printer takes input data as CAD solid model. It converts into STL file. By the application of G-codes printing, sciaky's electron beam (EB) gun deposits the metal layer by layer one over the other via the dual wire feed stock and an electron beam as a heat source to produce a required part inside a vacuum chamber. Once the part reaches required shape, it will be going to finish heat treatment and machining process. The process itself is measurable for components from minimum thickness from millimeters to max multiple meters in size, but it would be only limited by the size of the vacuum chamber. The diagrammatic representation and real model of electron beam gun and wire feeder shown in the Figure 2.

Sciaky's electron beam metal 3D printing technology is special kind metal additive
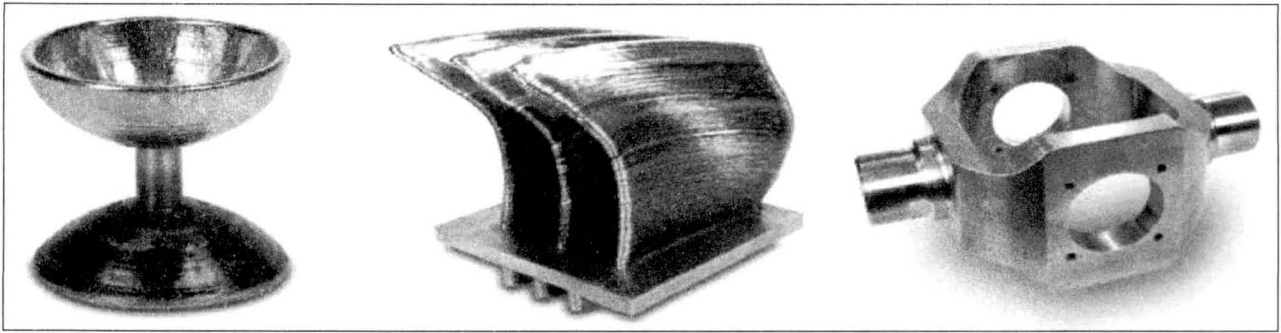
Fig. 3. (Source: sciaky.com).

manufacturing processes. It produces large-scale, high value metal parts. It can take so many months to complete and produce high quality products made of titanium, tantalum and nickel based alloys in a matter of days with very little material waste. It is starting with the 3D solid model from a CAD program. Sciaky's electron beam gun deposits metal layers one over other, until the part reaches final shape and is ready for finish machining. It inter layer real time imaging and sensing system ensures process repeatability and traceability (real-time adaptive control) provides consistent part geometry, mechanical properties, microstructure, metal chemistry and more from the initial stage of printing to the final. The gross deposition rates range from 3.18 to 11.34 kg of metal per hour. As compared to other metal 3D printing technologies, sciaky's Electron beam 3D printing technology is the best and unique benefits with dual wire feed system producing large, high quality metal parts. It is cost effective with high deposition rate. This technology provided to combine two different metal alloys into a single melt pool, managed with independent program control to create 'custom alloy' parts or ingots. It is also have the option to change the mixture ratio of the two materials, depending upon the required features of the parts and structures (Sciaky.com). Sciaky's brings together both quality and control in one step with IRISS. It is the Inter layer Real-time Imaging and Sensing System. IRISS is the only real-time adaptive control system in the market and it can sense and digitally self adjust metal deposition with precision and repeatability. The IRISS real-time closed-loop control is integrated with Sciaky's EBAM 3D-printing systems. Digital parameter control and adjustments are made in response to real-time measured data, without the process disruption. It records every second of deposition, so that the entire build can be reviewed, verifying consistency and keeping a record for later review. Prevents surprises by

dynamically adjusting parameters to maintain part integrity. Better insures net shape fabrication and reduces post processing time and costs such as machining and inspection. 3D printed parts shown below Figure 3.

Build volume

The build volume of final parts and structures may be up to 19 ft. x 4 ft. x 4 ft. (5.79 m x 1.22 m x 1.22 m) or round parts up to 8 ft. (2.44 m) in diameter can be produced with Sciaky's electron beam 3D printing machines. It can also be effective for smaller scale parts starting around 8 in ^{3} (203^3 mm).

Materials

The best materials for electron beam 3D printing metals are available in wire feed stock. These materials includes, niobium, inconel 718, 625, tantalum, tungsten, stainless steels, 2319, 4043 aluminum, titanium alloys, 4340 steel, 70-30 copper nickel and 70-30 nickel copper,

Applications

Sciaky's electron beam additive manufacturing methodology reduces lead times, material costs and machining times up to 80% as compared to conventional manufacturing. It is the fastest most cost-effective additive manufacturing process in the market for producing large metal parts. Inter layer real time imaging and sensing system is a patented with closed loop control technology. It ensures process repeatability and traceability (real-time adaptive control). The widest range of material options for large scale metal applications. Sciaky offers the greatest build envelope in the world for 3D printed metal parts. EBAM's solely dual wire feed process permits you to cater two different metal alloys into a single melt pool to create parts made

Material	Physical Characteristics	Molding Performance	Chemical Composition
Stainless Steel (316L)	Grain Size 15~53μm, Shape Spherical, Mobility 40S (Hall flow meter), Apparent density 3.9 g/cm³	Relative Density≥99%, Density 7.89 g/cm³, Tensile Strength≥560 M Pa, Yield strength≥480 M Pa, Elongation at break10~20 %, Elastic Modulus 180 G Pa, Hardness 158 HB	Fe (Balance) Cr (16~18%) Ni (10~14%) Mo (2~3%) Mn (≤2%) Si (≤1%) C (≤0.03%) P (≤0.0045%) H (≤120ppm) S (≤0.03%) O (≤0.13%)
Die Steel (MS1)	Grain Size 15~53μm, Shape Spherical, Mobility 40S (Hall flow meter), Apparent density 4.3 g/cm³	Relative Density≥99%, Density 8 g/cm³, Tensile Strength≥1090 M Pa, Yield strength≥1000 M Pa, Elongation at break10 % (thermal process : 4%), Elastic Modulus 160 G Pa (thermal process : 180 G Pa), Hardness 323 HB (thermal process : 585 G Pa)	Fe (Balance), Cr (8.5~9.5%), Ni (17~19%) , Mo (4.2~5.2%), Mn (≤0.1%) , Ti (≤0.8~0.9%), C (≤0.03%) Al (≤0.05~0.15%), S (≤0.01%) O (≤0.15%)
Titanium Alloy (TC4)	Grain Size 15~45μm, Shape Spherical, Mobility 45S (Hall flow meter), Apparent density 2.5 g/cm³	Relative Density≥99.9%. Density 4.51 g/cm³, Tensile Strength≥1000 M Pa, Yield strength≥900 M Pa, Extensibility≥4~10%, Elastic Modulus 100~120 G Pa, Hardness 294 HB	Ti (Balance), Al (5~6.75%), V (3.5~4.5%), Fe (≤0.3%), C (≤0.1%), Si (≤0.12%), O (≤1300ppm), N (≤400ppm),H (≤120ppm), Other (≤0.4%)
Aluminium Alloy (Al-Si₁₀Mg)	Grain Size 15~53μm, Shape Spherical, Mobility 150S (Hall flow meter), Apparent density1.45 g/cm³	Relative Density≥95%, Density 2.67 g/cm³, Tensile Strength≥330 M Pa, Yield strength≥245 M Pa, Elongation at break6 %, Elastic Modulus70 G Pa, Hardness120 HB	Al (Balance), Si (9~10%), Mg(0.2~0.45%), Cu (≤0.05%), Mn (≤0.45%), Ni (≤0.05%), Fe (≤0.55%), Ti (≤0.15%), O(≤0.15%)
Co-Cr Alloy (MP1)	Grain Size 15~53μm, Shape Spherical, Mobility 45S (Hall flow meter), Apparent density 4.2 g/cm³	Relative Density≥99%, Density 4.2 g/cm³, Tensile Strength≥1000 M Pa, Yield strength≥900 M Pa, Elongation at break 10 %, Elastic Modulus: 200 G Pa, Hardness 323~428 HB	Co (Balance), Cr(22~23%), Mo (5~10%), W (5~10%), Si (≤1.5%), C (≤0.03%), O (≤0.13%)
Ni-base Super alloy (IN718)	Grain Size15~53μm, Shape Spherical, Mobility 45S (Hall flow meter), Apparent density 4.4 g/cm³	Relative Density ≥99%, Density 8.15 g/cm³, Tensile Strength≥980 M Pa (thermal process : 1240 M Pa), Yield strength≥700 M Pa (thermal process : 1000 M Pa), Elongation at break12~30 %, Elastic Modulus140~180 G Pa, Hardness283 HB (thermal process : 455 HB)	Ni(50~55%,,Fe(Balance, Cr(17~22%), Nb(4.75~5.5%O, Mo(2.8~3.3%), Ti(0.65~1.15%) Co(≤1%) Al(0.2~0.8%), Si(≤0.35%), C(≤0.08%), P(≤0.015%)
Chromium Bronze(QCr1)	Grain Size15~53μm, Shape: Spherical, Mobility 50S (Hall flow meter), Apparent density 4.8 g/cm³	Relative Density≥98%, Density 8.9 g/cm³, Tensile Strength 300 M. Pa, Yield strength 200 M Pa, Elongation at break 5 %, Elastic Modulus 90 G Pa, Hardness 170~200 HB	Cu(Balance), Cr(0.5~1.5%), Zr(0.04~0.1%), Mg(0.04~0.08%)

of custom alloys. It also permits designers to varying alloy mixtures to manufacture different graded parts. Graded parts can also be produced by switching from thin wire for fine deposition and to thick wire for gross deposition feedstock. EBAM works exceptionally well with refractory alloys and produces notably less material waste. The wire feedstock is importantly less expensive than powder feedstock. It is easier to store, and it isn't highly flammable like some powder feed stocks. With EBAM's pure vacuum environment, the process does not require the use of Argon or any inert gas for part shielding. Start 3D printing parts in as little as 12 minutes; While EBAM pump down times can vary by chamber size and application, it is still, by far, the fastest metal AM process in the market when you consider EBAM's industry-leading high deposition rate.

2. Conclusions

1. Sciaky's electron beam additive manufacturing reduces the time and cost associated with traditional manufacturing.
2. It reduces lead times, material cost by up to 80%.
3. It is world's fastest metal deposition 3D printing technology with high deposition rate.
4. It is the best methodology to provide good quality products and true scalability for part sizes.

Acknowledgements

References

Anderson, E. (2013). Additive Manufacturing in China: Threats, Opportunities, and Developments (Part 1). *SITC Bulletin Analysis*, 1–5.

Arcam AB (2014).*www.arcam.com*.

Bhavar, V., Kattire, P., Patil, Vinaykumar, Khot, Shreyans, Gujar, Kiran, & Singh, R. (1-2 September, 2014). *A review on powder bed fusion technology of metal additive manufacturing*. 4th International conference and exhibition on Additive Manufacturing Technologies-*AM-2014 (Bangalore)*.

Chua, C. K., Leong, K. F. & Lim, C. S. (2010). *Rapid Prototyping: Principles and Applications*. World Scientific Publishing: Singapore, Ed 3.

Cooper, K. P. (6 March, 2014). *Laser-based additive manufacturing: where it has been, where it needs to go*. Proceedings of SPIE - The International Society for Optical Engineering. 10.1117/12.2044255.

Herderick E. (16-20 October, 2011). *Additive Manufacturing of Metals: A Review*. Materials Science and Technology (MS&T) 2011. Columbus, Ohio.

https://www.sciaky.com

Lu, Z. L, Cao, J. W., Jing, H., Liu, T., Lu, F., Wang, D. X. & Li, D. C. (2013). Review of main manufacturing processes of complex hollow turbine blades. *Virtual and Physical Prototyping*, 8(2), 87–95.

Quail, F., Stickland, M., & Scanlon, T. J. (2009). Rapid manufacturing technique used in the development of a regenerative pump impeller. *Rapid Prototyping Journal*, 16(5).

Sun, C. N. & Wei, J. (2013). *3D Additive Manufacturing*. In SIM Tech Annual Manufacturing Forum.

G. Kishan is working as a faculty of Mechanical Engineering, University College of Engineering & Technology for Women, Kakatiya University Warangal. He got his M.E (CAD/CAM) from Osmania University, Hyderabad, His research area of interest are Metal working processes, Natural fiber composites, CAD, CAM, FEA, Solid modeling, 3 Printing, Digital manufacturing and multidisciplinary approach. He has 6 years experience in teaching of Engineering Mechanics, strength of materials and Engineering Drawing; He published 8 papers in reputed journals.

Investigation on corrosion resistance of 316 γ stainless steel clad constructional steel

Jaydeep Mondal, Manas Kumar Saha, Santanu Das*

Kalyani Government Engineering College, Kalyani, West Bengal, India.

ABSTRACT

Surfaces of structural members usually degrade under corrosion causing reduction in service life. This results in increased cost involving preventive methods or/and rework. Cladding is one such method for preventing this problem to some extent. Desired weld quality for gas metal arc welding process, a well-accepted method for developing clad layer and overlays, can be achieved by selecting appropriate process parameters. In the present investigation, gas metal arc welding is applied to develop 316 γ stainless steel clad layer on E350 constructional steel base plate with varying welding current and torch travel speed. Results indicate lowering of corrosion rate with increasing welding current and arc travel speed at a constant travel speed and constant current respectively. No clear trend of change in corrosion rate with the variation of heat input is seen. However, austenitic stainless steel cladding is found to improve corrosion resistance remarkably to apply to industry effectively.

1. Introduction

High strength and corrosion resistant structural members are the basic requirement in many engineering applications. Cladding is a popular surfacing technique used for improving corrosion resistance of structural members, which are exposed to hostile environment. It is a process of depositing thick layer of corrosion resistant material on corrosion prone mother materials layer by layer fashion. In recent years, weld cladding processes have been developed rapidly and are now applied in numerous industries such as chemical, fertilizer, nuclear and steam power plants, food processing, and petrochemical industries (Saha & Das, 2016; Saha & Das, 2018; Liu et al., 2017; Gorunov et al., 2018; Walters et al., 2018; Lailatul et al., 2017).

Various welding processes employed for cladding are shielded metal arc welding, submerged arc welding, gas tungsten arc welding, plasma arc welding, laser beam welding, gas metal arc welding, flux cored arc welding, electroslag welding, oxy-acetylene welding, explosive welding, etc. Among the processes employed for weld cladding, GMAW is widely accepted by the industries due to its various advantages over the other processes

i.e. high reliability, capability in performing in all positions, high rate of deposition, high productivity, no flux, low cost, etc. (Prajapati et al., 2018; Joseph et al., 2019; Balan et al., 2018; Saha et al., 2012; Mondal et al., 2016; Kannan & Murugan, 2006; Prabhu & Alwarsamy, 2017).

The desirable characteristics of cladding alloy are reasonable strength, weldability, resistance to corrosion, etc. The material, which possesses good corrosion resistance, oxidation resistance, erosion resistance property, is used for cladding on corrosion prone low alloy steel substrate for better mechanical properties and long life. Duplex stainless steel, super duplex stainless steel shows better corrosion resistance properties as well as mechanical strength, though they are the costly alternative cladding materials. However, due to high amount of chromium, nickel and molybdenum, austenitic stainless steel also exhibits good corrosion resistance in chloride environment (Saha et al., 2018; Eghlimi et al., 2014; Kaushal et al., 2018; Saha et al., 2018; Verma et al., 2013). Moreover, cost involves against austenite cladding is comparatively less.

Welding parameters play an important role on corrosion resistance characteristics. The main problem faced in cladding with austenitic stainless steel is the selection of the appropriate process parameters for achieving the required

*Corresponding author,
E-mail: sdas.me@gmail.com

quality of cladding. Process parameters such as welding current, arc voltage, torch travel speed, tip-to-nozzle distance, torch angle, gas flow rate, composition of shielding gas, heat input, etc. for a particular welding method for a particular set of work materials (base and cladding materials) play most vital role for physical and chemical and metallurgical properties (Chakraborty et al., 2013; Sabiruddin et al., 2013; Besliu et al., 2017; Om & Pandey, 2013; Gharibshahiyan et al., 2011; Khamari et al., 2019). Thickness of the workpiece also plays an important role in gas metal arc welding process (Elmer et al., 1989). To control quality of cladding engineers are very much curious to know the effect of these process parameters on the desired properties. To minimize the corrosion rate of γ steel cladding on E350 constructional steel, it is important to know the effect of heat input and its main contributor parameters namely welding current and arc travel speed on corrosion rate of clad part. Minimization of corrosion rate can minimize maintenance and rework, increase service life of the component and so also the profit.

In this work, an experimental study is carried out on corrosion resistance performance of austenitic (γ) stainless steel (316) cladding on 25 mm thick E350 steel plate with three different sets of welding currents and three different sets of travel speeds keeping constant welding voltage in gas metal arc welding process with 100% CO_2 as shielding gas.

2. Experimental Work

In this work, cladding was performed with ESAB India Ltd. made GMAW setup of Model No. Auto K 400 with 60% duty cycle. Austenitic stainless steel (316) filler wire is used as wire electrode material for cladding on low alloy structural steel (E350) plate of size 70mm x 60mm x 25mm. 316 γ stainless steel contains 70.95% Iron, 15.05% chromium, 9.94% nickel, 2.09% molybdenum, 1.102% silicon, 0.34% copper, 0.076% carbon with small amount of phosphorus, sulfur, cobalt, niobium, titanium, vanadium, tungsten, selenium, strontium, etc. On the other hand E350 low alloy steel contains 98.95% iron, 0.412% manganese, 0.192% silicon, 0.146% carbon with trace amount of phosphorus, sulfur, chromium, molybdenum, nickel, cobalt, copper, niobium, titanium, vanadium, tungsten, lead, tin, tantalum, boron, etc. Carbon equivalent, C_{eq} for the base material E 350 is found to be nearly 0.235. Carbon equivalent;

C_{eq} for austenitic stainless steel (316) is found to be nearly 4.38.

2.1 Experimental procedure

First, the base materials are made rust free and clean. During cladding with 316 filler wire, 50% overlap of the beads was taken using GMAW setup. This is done by positioning the filler wire at the toe of the previous bead. The heat input of welding is calculated by using the equation (1).

$$Q = \frac{V \times I \times 60}{S \times 1000} \times \eta \tag{1}$$

Where, V is Welding voltage (V), I is Welding current (A), S is Travel speed (mm/min), Q is Heat Input (kJ/mm) and η is efficiency of GMAW and in the current work, it is taken as 0.8.
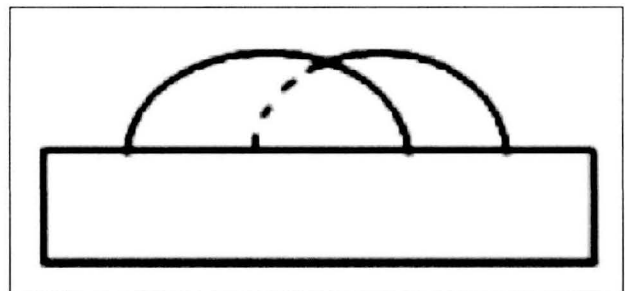

Fig. 1. Schematic diagram of 50% overlap.

2.2 Sample preparation

After cladding test, samples are cut by an abrasive cutter with approx. 10x10mm² surface area of cladded face. Then the cladded faces are made flat with grinding. Then these samples were used for hardness test, corrosion test and microstructural study.

2.3 Corrosion test

First, the samples are polished and weighed by digital weighing machine (Model: M K 100E, Petit Balance) with capacity of 100g and a readability upto 0.001g. Then, the test samples are coated by the Teflon tapes, leaving only the cladded area exposed and each sample is immersed in a corrosive medium for 24 hours. The corrosive medium is prepared with 29g ferric chloride, 24 cc HCl and 76 cc distilled water. After removing from the corrosive medium, the test samples are cleaned with water and then weighed again. The weight losses by the corrosive medium are found by the difference of initial and final weight

Table 1

Process parameters of cladding done by austenitic stainless steel electrode [316].

Test Sample No.	Weld Current (A)	Travel Speed (mm/min)	Weld Voltage (V)	Corresponding Heat Input (kJ/mm)
1	140	392		0.462
2	140	362		0.501
3	140	325		0.558
4	170	392		0.562
5	170	362		0.608
6	200	392	27	0.661
7	170	325		0.677
8	200	362		0.716
9	200	325		0.797

Table 2

Results of corrosion test of base plate E350.

Sl. No.	Base Plate	Area (mm²)	Weight Loss (gm)	Corrosion Rate (gm/m²hr)
1	Low alloy steel E350	10.8×10.7	1.257	453.22

Table 3

Results of corrosion test of austenitic stainless steel cladded test samples of two replications.

Sample	Heat input kJ/mm	1st Replications (Test Duration= 24 hr)			2nd Replications (Test Duration= 24 hr)			Average Corrosion Rate (g/m²hr)
		Exposed Area (mm²)	Weight Loss (g)	Corrosion Rate (g/m²hr)	Exposed Area (mm²)	Weight Loss (g)	Corrosion Rate (g/m²hr)	
1	0.462	10×10.1	0.365	150.57	10×10.5	0.450	178.57	164.57
2	0.501	10.2×9.8	0.380	158.39	10.5×10.5	0.497	187.83	173.11
3	0.558	10.3×10.5	0.468	222.34	10.5×10.8	0.489	179.67	179.98
4	0.562	10.5×10	0.402	159.52	10×10.1	0.372	153.46	156.49
5	0.608	10.1×9.8	0.413	173.85	10.8×10.9	0.462	163.52	168.69
6	0.661	10.4×10.5	0.385	146.90	10.3×10.7	0.407	153.87	150.38
7	0.677	10.5×10	0.482	191.26	10×10.9	0.412	157.49	174.38
8	0.716	9.5×10	0.347	152.19	10.2×10.2	0.397	158.99	155.59
9	0.797	10.1×10.8	0.414	158.14	10.5×10.5	0.408	154.19	156.16

of the test samples. Corrosion rate is found by weight loss (w in g) from unit cross section exposed area (A in m²) per unit time (T in hr).

2.4 Microstructural study

Test samples are ground on a belt grinder using 60, 80 and 120 grades of emery belts. Then, these samples are polished by using five different grades of emery paper (180, 400, 800, 1000 and 1200) and finally on velvet cloth using alumina suspension as abrasive to obtain mirror finish in the rotating disc grinding machine. The samples are etched by combination of Waterless Kalling's reagent (100cc ethanol, 100cc HCl and 5g $CuCl_2$) and Ralph's reagent (100cc water, 200cc Methyl Alcohol, 100cc HCl, 5cc HNO_3, 2g $CuCl_2$, 7g $FeCl_2$). Waterless Kalling's reagent reacts with austenitic stainless steel to reveal the fusion boundary of cladded specimens. These samples are observed under metallurgical microscope (Make: Meitzer, India, Model: BM/MIEZS) at 200x magnification.
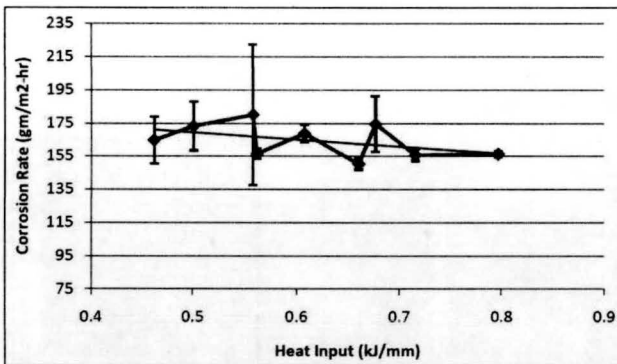
Fig. 2. Corrosion rate of 316 austenite stainless steel cladding on low alloy steel in different heat input.
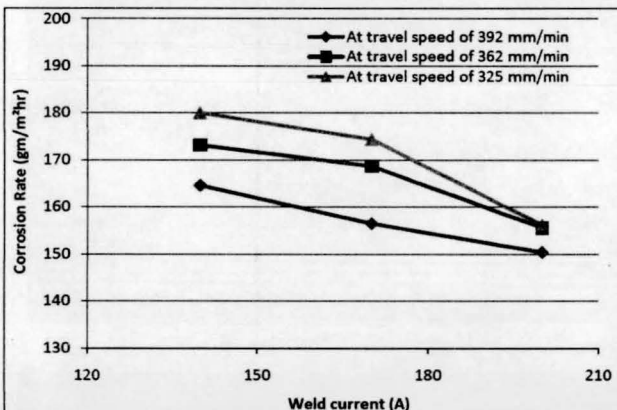

Fig. 3. Plot of average corrosion rate with welding current at constant travel speed of austenitic stainless steel cladded test samples of two replications.
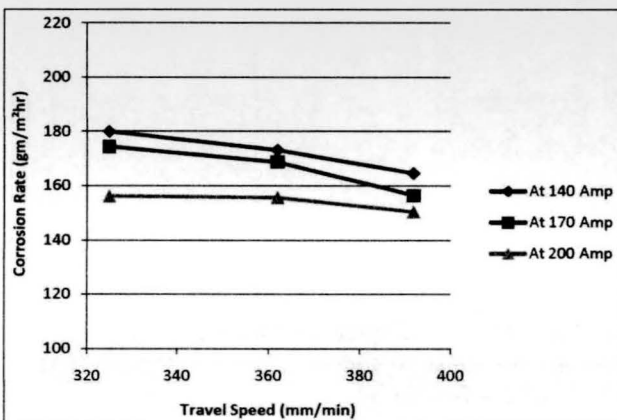

Fig. 4. Plot of average corrosion rate with travel speed at constant welding current of austenitic stainless steel cladded test samplesof two replications.

The process parameters selected for cladding are shown in Table 1.

3. Results and Discussion

Table 2 and Table 3 show the results of corrosion test obtained from base plate (E350) cladded test samples respectively.

Table 3 shows corrosion rate of austenitic stainless steel cladded test samples of different welding parameters. The corrosion rate found at base plate E350 is 3 times the least corrosion rate found in the austenitic stainless steel cladded test sample, and 2.7 times the average corrosion rate of austenitic stainless steel cladded test samples. Austenitic stainless steel electrode also contains appreciable amount of chromium, nickel and molybdenum, which can be the main cause behind this corrosion resistive property.

Based on results from corrosion test of clad parts during both replications, plot of change in corrosion rate against change in heat input is constructed in Fig. 2. From Fig. 2, it can be stated that heat input does not have substantial influence on corrosion rate of austenitic stainless steel cladded E350 low carbon steel specimens. Fig. 2 also shows that except one case (point 3), deviations of corrosion rate during two replicated experiment are less.

The results tabulated in Table 3 are plotted in Fig. 3 and Fig. 4 to observe change in corrosion rate with weld process parameters such as current and travel speed. In this approach, firstly change of corrosion rate at three constant travel speeds are plotted against change in current, keeping arc voltage constant throughout the experiment. Secondly, the corrosion rates at three constant currents are plotted against torch travel speed, keeping arc voltage constant for each time.

Effects of welding current on corrosion rate are shown in Fig. 3. This figure clearly indicates the decreasing tendency of corrosion rate with an increase in current at a constant travel speed within experimental domain. Corrosion rate also shows decreasing tendency with increasing travel speed. Lowest corrosion rate is observed at highest current corresponding to maximum travel speed within experimental domain.

The effects of welding travel speed on corrosion rate are shown in Fig. 4. The constant welding current line has similar tendency towards corrosion rate. Corrosion rate decreases with increasing travel speed keeping weld current and voltage constant.

3.1 Microstructure of cladding

Observation of microstructure of the clad portion is made under a metallurgical microscope. The Ralph's reagent and Waterless Kalling's reagent
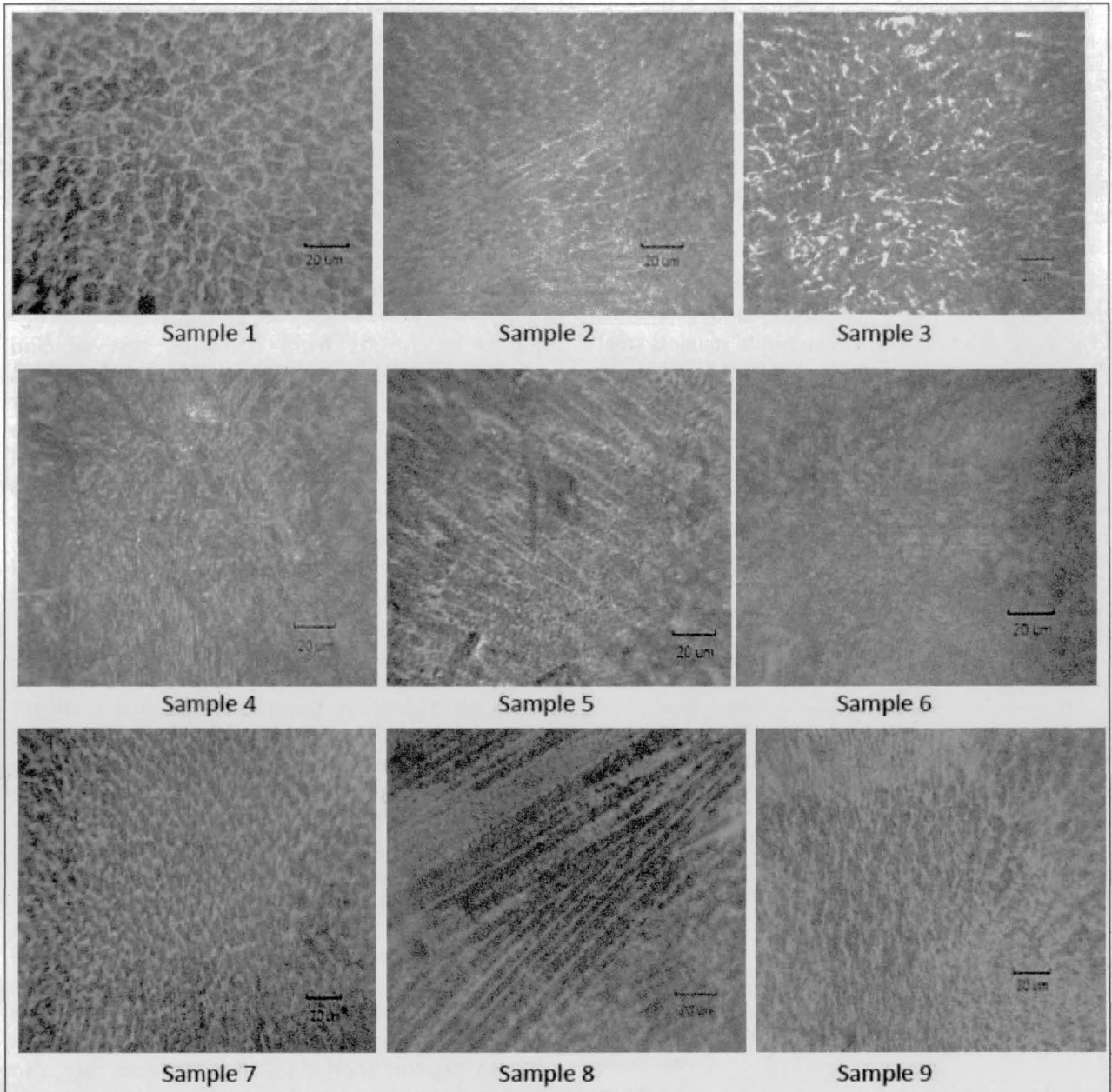
Fig. 5. Microstructure of clad samples of 1st replication (200x).

are used as etchant. The magnification is taken as 200X except Fig. 5 that contain the photograph of corroded surface of duplex and austenitic cladded test samples after corrosion test with a magnification of 4X.

Formation of different phase in clad portion is possible during the phase transformation when cooling. The grain growth and final phase mostly depend on the solidification rate and alloy content. Elmer et al. (1989) described five solidification modes of stainless steel alloys as follows:

Single phase austenite (A)
Primary austenite with second phase ferrite (AF)

Eutectic ferrite and eutectic austenite (E)
Primary ferrite with second phase austenite (FA)
Single phase ferrite (F)

Microstructures of austenitic clad specimens are shown in Fig. 5. In Fig. 5, sample 1 through sample 9 show the cellular and epitaxial growth of austenite with intercellular ferrite and form primary austenite with second phase ferrite (AF) microstructure of austenitic stainless steel cladded test samples. Various intermetallic phases are also found in the microstructures.

The austenite equivalent is determined from the concentrations of austenite formers Ni, C, and Mn.
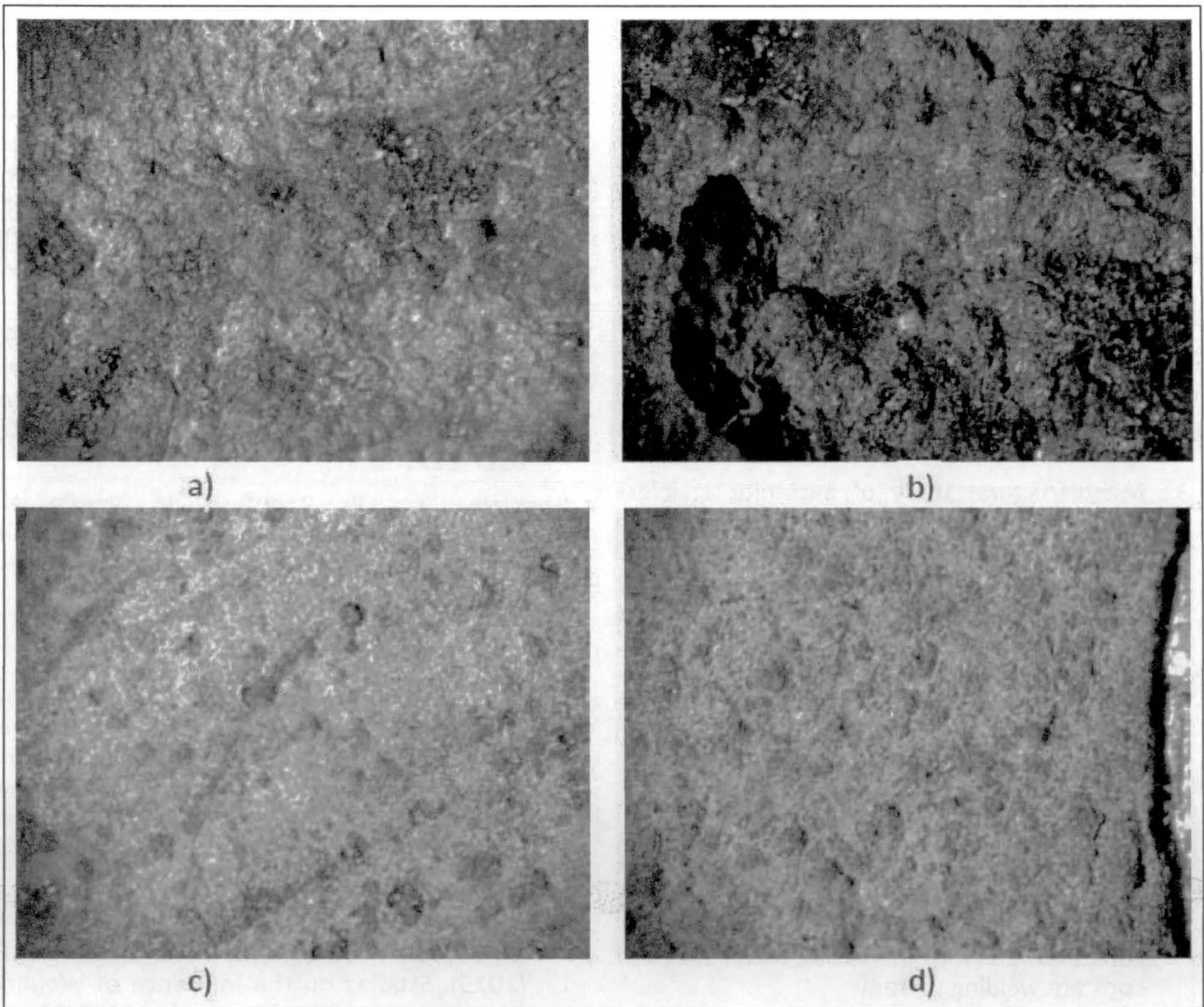
Fig. 6. (a-d). Photograph of corroded surface of cladded zone after corrosion test of austenitic stainless steel cladded test.

Austenite stainless steel electrode contains 0.0758% C, 1.01% Mn, 9.93% Ni. Nickel has an fcc structure, thus favouring the fcc structure of austenite and known as austenite former. DeLong (1974) demonstrated nitrogen to be a strong austenite former, and refined Schaeffler's (1949) equation to evaluate chromium equivalent and nickel equivalent as shown in equation (2) and (3) respectively.

Nickel equivalent = % Ni + 30 × (% C + % N) + 0.5 × % Mn 　　　　　　　　　　　　　　　　(2)

Chromium equivalent = % Cr + %Mo + 1.5(% Si) + 0.5(% Nb) + 2(% Ti) 　　　　　　　　　(3)

For 316 austenite stainless steel electrode, chromium and nickel equivalent are 17.43 and 12.76 respectively. Due to high nickel equivalent, it solidifies as single phase austenite. At higher heat input, solute redistribution takes place, and ferrite precipitates from austenite. Decrease in austenite phase and/or increasing ferrite phase decrease corrosion rate as shown in the present work.

Photographs of corroded surface after corrosion test of austenitic stainless steel cladded test samples are shown in Fig. 6.

Fig. 6(a-d) show the corroded surface with few corrosion pits along with general corrosion occurring at the corroded surface.

4. Conclusions

On the basis of present experimental investigation regarding performance of cladding with austenitic stainless steel on low alloy steel by GMAW, following conclusions may be drawn:

1. Corrosion rate of E350 base plate is observed to be more than 3 times than the respective minimum corrosion rate conditions and 2.7 times the average corrosion rate of austenitic stainless steel cladded test samples. Corrosion test results obtained from austenitic stainless steel cladding does not indicate any remarkable influence on corrosion rate with heat input. The least corrosion rate is found at higher heat input of 0.661 kJ/mm applying 200 A weld current, 392 mm/min travel speed and 27 V weld voltage.

2. There is no significant change in corrosion rate against change in heat input within experimental domain.

3. Microstructural study of austenitic stainless steel shows the cellular and epitaxial growth of austenite with intercellular ferrite and form primary austenite with second phase ferrite (AF) microstructure. Austenite stainless steel electrode contains 0.0758% C, 1.01% Mn, 9.93% Ni. Nickel has an fcc structure, thus favouring the fcc structure of austenite and known as austenite former. Due to high nickel equivalent, it solidifies as single phase austenite with intercellular ferrite structure.

4. The result indicates that corrosion rate decreases with increasing current at constant travel speed within experimental. On the other hand, there has a decreasing tendency of corrosion rate with increasing travel speed at constant welding current.

References

Balan, A. V., Shivasankaran, N., & Magibalan, S. (2018). Optimization of cladding parameters for resisting corrosion on low carbon steels using simulated annealing algorithm. *Materials Research Express,* 5(4), 046527. DOI: 10.1088/2053-1591/aab7cb.

Besliu, M. M., Voiculescu, I., & Solomon, G. (2017). Effects of dilution on weld overlays realized with flux-cored arc welding (FCAW) process using 309LV filler metal on the S235JR steel. *U.P.B. Scientific Bulletin, Series B,* 79(1), 173-182.

Chakraborty, B., Das, H., Das, S., & Pal, T. K. (2013). Effect of process parameters on clad quality of duplex stainless steel using GMAW process. *Transactions of the Indian Institute of Metals,* 66(3), 221-230. DOI: 10.1007/s12666-013-0246-x.

Delong, W. T. (1974). Ferrite in austenitic stainless steel weld metal. *Welding Journal,* 53(7), 273s-286s.

Eghlimi, A., Shamanian, M., & Raeissi, K. (2014). Effect of current type on microstructure and corrosion resistance of super duplex stainless steel claddings produced by the gas tungsten arc welding process. *Surface Coating Technology,* 244, 45-51. DOI: 10.1016/j.surfcoat.2014.01.047.

Elmer, J. W., Allen, S. M., & Eager, T. W. (1989). Microstructural development during solidification of stainless steel alloys. *Metallurgical Transactions A,* 20A(10), 2117-2131.

Gharibshahiyan, E., Raouf, A. H., Parvin, N., & Rahimian, M. (2011). The Effect of Microstructure on Hardness and Toughness of Low Carbon Welded Steel using Inert Gas Welding. *Journal of Materials and Design,* 32, 2042–2048.

Gorunov, A. I., Nyukhlaev, O. A., & Gilmutdinov, A. K. (2018). Investigation of microstructure and properties of low-carbon steel during ultrasonic-assisted laser welding and cladding. *International Journal of Advanced Manufacturing Technology,* 99, 2467–2479. DOI: 10.1007/s00170-018-2620-7.

Joseph, G.B., Valarmathi, T.N., Mageshwaran, G., Jeevahan, J., Sriram, V., & Durai, R.R.B. (2019). Studies on the Influence of Welding Parameters in Cladding of ERNiCrMo-10 on AISI 4140 Using GMAW Process. *Advances in Manufacturing Technology. Lecture Notes in Mechanical Engineering,* Springer, Singapore. 615-621. DOI: 10.1007/978-981-13-6374-0_67.

Kannan, T., & Murugan, N. (2006). Effect of flux cored arc welding process parameters on duplex stainless steel clad quality. *Journal of Materials Processing Technology,* 176, 230–239.

Kaushal, S., Gupta, D., & Bhowmick, H. (2018). On surface modification of austenitic stainless steel using microwave processed Ni/Cr_3C_2 composite cladding. *Surface Engineering,* 34(11), 809-817. DOI: 10.1080/02670844.2017.1362808.

Khamari, B. K., Karak, S. K., & Biswal, B. B. (2019). Relation between different process parameters in gas metal arc welding. *Indian Welding Journal,* 52(2), 44-55. DOI:10.22486/iwj.v52i2.181779.

Lailatul, P. H., & Maleque, M. A. (2017). Surface modification of duplex stainless steel with SiC preplacement using TIG torch cladding. *Procedia Engineering*, 184, 734-782. DOI: 10.1016/j.proeng.2017.04.151.

Liu, J., Yu, H., Chen, C., Weng, F., & Dai, J. (2017). Research and development status of laser cladding on magnesium alloys: a review. *Optics Lasers Engineering*, 93, 195-210. DOI: 10.1016/j.optlaseng.2017.02.007.

Mondal, A., Saha, M. K., Hazra, R., & Das, S. (2016). Influence of heat input on weld bead geometry using duplex stainless steel wire electrode on low alloy steel specimens. *Cogent Engineering*. 3(1), 1143598/1-14. DOI: 10.1080/23311916.2016.1143598.

Om, H., & Pandey, S. (2013). Effect of Heat Input on Dilution and Heat Affected Zone in Submerged Arc Welding Process. *Sadhana*, 38(6), 1369–1391. DOI: 10.1007/s12046-013-0182-9.

Prabhu, R., & Alwarsamy, T. (2017). Effect of process parameters on ferrite number in cladding of 317L stainless steel by pulsed MIG welding. *Journal of Mechanical Science and Technology*, 31, 1341-1347. DOI: 10.1007/s12206-017-0234-x.

Prajapati, P., Badheka, V. J., & Mehta, K. P. (2018). Hybridization of filler wire in multi-pass gas metal arc welding of SA516 Gr70 carbon steel. *Materials and Manufacturing Processes*. 33(3), 315-322. DOI: 10.1080/10426914.2016.1244847.

Sabiruddin, K., Bhattacharya, S., & Das, S. (2013). Selection of appropriate process parameters for gas metal arc welding of medium carbon steel specimens. *International Journal of Analytical Hierarchy Process*, 5(2), 252-266. DOI: 10.13033/ijahp.v5i2.184.

Saha, M. K., & Das, S. (2016). A Review on Different Cladding Techniques Employed to Resist Corrosion. *Journal of the Association of Engineers*, 86(1-2), 51–63. DOI: 10.22485/jaei/2016/v86/i1-2/119847.

Saha, M. K., & Das, S. (2018). Gas Metal Arc Weld Cladding and its Anti-Corrosive Performance- A Brief Review. *Athens Journal of Technology and Engineering*, 5(2), 155-174. DOI: 10.30958/ajte.5-2-4.

Saha, M. K., Das, S., & Bandyopadhyay, A. (2012). Application of L6 orthogonal array for optimal selection of some process parameters in GMAW process, *Indian Welding Journal*, 45(4), 41-50. DOI: 10.22486/iwj.v45i4.141203.

Saha, M. K., Hazra, R., Mondal, A., & Das, S. (2018). Effect of heat input on geometry of austenitic stainless steel weld bead on low carbon steel. *Journal of Institution of Engineers (India), Series C,* 100(4), 607-615. DOI 10.1007/s40032-018-0461-7.

Saha, M. K., Mondal, A., Hazra, R., & Das, S. (2018). Anticorrosion performance of FCAW cladding with regard to the influence of heat input. *Journal of Welding and Joining,* 36(5), 61-69. DOI 10.5781/JWJ.2018.36.5.8.

Saha, M. K., Mondal, J., Mondal, A., & Das, S. (2018). Influence of heat input on corrosion resistance of duplex stainless steel cladding using flux cored arc welding on low alloy steel flats. *Indian Welding Journal,* 51(3), 66-72. DOI:10.22486/iwj.v51i3.175002.

Schaeffler, A. L. (1949). Constitution diagram for stainless steel weld metal. *Metal Progress,* 56(5), 680-680B.

Verma, A. K., Biswas, B. C., Roy, P., De, S., Saren, S., & Das, S. (2013). Exploring quality of austenite stainless steel clad layer obtained by metal active gas welding. *Indian Science Cruiser,* 27(4), 24-29. DOI:10.24906/isc/2013/v27/i4/177608.

Walters, W. S., Durham, P., & Hodge, N. A. (2018). The adsorption and desorption of water from a carbonaceous deposit layer on the surface of stainless steel representing spent AGR nuclear fuel cladding. *Journal of Nuclear Science Technology,* 55(4), 374-385. DOI: 10.1080/00223131.2017.1403384.

Jaydeep Mondal is presently working as a faculty in Mechanical Engineering Department at Camellia Institute of Technology, Madhyamgram, Kolkata, West Bengal. He obtained bachelor degree in Mechanical Engineering from Jalpaiguri Government Engineering College, West Bengal in 2008 and completed his post graduation in Production Engineering from Kalyani Government Engineering College, West Bengal in 2016. He has 4 years of teaching experience and published a paper in Indian Welding Journal in 2018. (E-mail: jdeep.mondal@gmail.com)

Manas Kumar Saha is presently working as a Lecturer in Mechanical Engineering at Engineering Institute for Junior Executives, Dalalpukur, Howrah, West Bengal. He previously served at Nazrul Centenary Polytechnic, Burdwan, West Bengal. He completed his undergraduate course in Mechanical Engineering from Jadavpur University, Kolkata and Masters' in Production Engineering from Kalyani Govt. Engineering College, Kalyani, West Bengal. He served Hindustan Motors, Hooghly, West Bengal for 9 years. He has submitted Ph.D thesis at Maulana Abul Kalam Azad University of Technology, West Bengal recently. He did his research work on Weld Cladding using GMAW and FCAW process. He presented and published 10 numbers of research Papers in International and National Conferences, 12 numbers of Journal Papers and 02 numbers of Book Chapters so far. He is a Life Member of The Indian Institute of Welding, The Association of Engineers, India as well as Institute of Science, Education and Culture. (E-mail: manassaha71@gmail.com)

Dr. Santanu Das is, at present, Professor and Head, Department of Mechanical Engineering, Kalyani Govt. Engineering College, Kalyani, West Bengal. He graduated and post graduated in Mechanical Engineering from Jadavpur University, Kolkata. He obtained Ph.D (Engineering) from IIT Kharagpur. He guided 08 Ph.D and 126 M.Tech theses, and 99 B.Tech projects in the area of machining, grinding, welding, coating, weld cladding, inventory management, etc. He is guiding 08 Ph.D research scholars. He has 160 publications in Journals and 23 in Book Chapters, and 91 in International and 159 in National Conferences. He was awarded 'Shiksha Ratna' in 2018 by Education Department, Govt. of West Bengal as an Outstanding Teacher. He delivered Engineer Soumitra Kumar De Memorial Lecture in 2019 as invited by Kolkata Branch of The Indian Institute of Welding. He received Production Division Award 2019 and Second Prize of Railway Board 2019 from The Institution of Engineers (India).